LOCKHEED MARTIN ENERGY RESEARCH LIBRARIES
3 4456 0514409 1

CENTRAL RESEARCH LIBRARY
DOCUMENT COLLECTION

OAK RIDGE NATIONAL LABORATORY
operated by
UNION CARBIDE CORPORATION
NUCLEAR DIVISION
for the
U.S. ATOMIC ENERGY COMMISSION

ORNL-TM- 3353

cy. 56

DATE - April 12, 1971

OAK RIDGE NATIONAL LABORATORY
CENTRAL RESEARCH LIBRARY
DOCUMENT COLLECTION
LIBRARY LOAN COPY
DO NOT TRANSFER TO ANOTHER PERSON
If you wish someone else to see this document, send in name with document and the library will arrange a loan.
UCN-7969 (3 3-67)

Neutron Physics Division

MUON TRANSPORT AND THE SHIELDING OF HIGH-ENERGY (≤ 500 GeV) PROTON ACCELERATORS*

R. G. Alsmiller, Jr., F. S. Alsmiller,
J. Barish, and Y. Shima†

Abstract

Calculated results on the muon shielding required around high-energy (200 GeV and 500 GeV) proton accelerator targets are presented. The calculations differ from those presented previously in that, in addition to the angular scattering of the muons due to Coulomb elastic collisions, an estimate of the angular scattering of the muons due to bremsstrahlung production, pair production, and nonelastic nuclear collisions is included. It is found that the angular scattering of the muons due to bremsstrahlung production, pair production, and nonelastic nuclear collisions does not have a pronounced effect on the shield dimensions and therefore for many design purposes may be neglected.

The calculations also differ from those presented previously in that the case of laminated shields is considered.

---

*To be presented at the International Congress on Protection Against Accelerator and Space Radiation, CERN, Geneva, April 26-30, 1971.

†Present address: Soreq Nuclear Research Center, Yavne, Israel.

NOTICE This document contains information of a preliminary nature and was prepared primarily for internal use at the Oak Ridge National Laboratory. It is subject to revision or correction and therefore does not represent a final report.

This report was prepared as an account of work sponsored by the United States Government. Neither the United States nor the United States Atomic Energy Commission, nor any of their employees, nor any of their contractors, subcontractors, or their employees, makes any warranty, express or implied, or assumes any legal liability or responsibility for the accuracy, completeness or usefulness of any information, apparatus, product or process disclosed, or represents that its use would not infringe privately owned rights.

MUON TRANSPORT AND THE SHIELDING OF HIGH-ENERGY (≤ 500 GeV) PROTON ACCELERATORS*

R. G. Alsmiller, Jr., F. S. Alsmiller, J. Barish**, and Y. Shima†

Neutron Physics Division
Oak Ridge National Laboratory
Oak Ridge, Tennessee, U.S.A.

1. INTRODUCTION

In the shielding of high-energy accelerators, it is often necessary to consider the transport of high-energy muons through matter. In several previous papers[1-3], the results of muon shielding calculations have been presented. In these papers, the energy loss of muons due to the ionization and excitation of atomic electrons, bremsstrahlung production, pair production, and nonelastic nuclear interaction was treated in the continuous slowing-down approximation, and it was assumed that the angular deflection of the muons was due entirely to Coulomb scattering from the nucleus. In this paper, shielding calculations similar to those obtained previously but which include an estimate of the angular deflection of the muons due to bremsstrahlung production, pair production, and nonelastic nuclear interaction are presented. The assumption that the energy loss of muons may be treated in the continuous slowing-down approximation is utilized in all of the calculations, and it is assumed that the angular deflection of the muons due to all physical processes may be treated in the small-angle multiple-scattering approximation of Eyges[4]. Since neither the continuous slowing-down approximation nor the small-angle multiple-scattering approximation is entirely valid for all of the scattering processes being considered, the calculated results must be considered to be very approximate[5]. At the very high energies considered here, the muon differential scattering cross sections that are needed in the calculations are only poorly known, and for this reason also the results must be considered to be very approximate.

*) Research funded by the U. S. Atomic Energy Commission under contract with Union Carbide Corporation.

**) Mathematics Division.

†) Present address: Soreq Nuclear Research Center, Yavne, Israel.

LOCKHEED MARTIN ENERGY RESEARCH LIBRARIES

The calculated results presented here also differ from those presented previously[1-3] in that the case of shields composed of layers of different materials is considered.

In Section 2 an approximate muon transport equation for a zero-width beam of muons normally incident on a laminated slab shield is derived, and the solution to the equation is discussed. In Section 3 the muon stopping powers and the differential cross-section data used in the calculations are presented. In Section 4 numerical results for 200-GeV and 500-GeV muons normally incident on both homogeneous and laminated slab shields are presented. In Section 5 the method used to calculate muon isodose curves in a homogeneous shield around a high-energy proton accelerator target is described. Results are given for a soil shield when 200- and 500-GeV protons are incident on a beryllium target and for an iron shield when 500-GeV protons are incident on a beryllium target. In both Sections 4 and 5 calculated results with the angular effects of bremsstrahlung production, pair production, and non-elastic nuclear scattering both included and neglected are presented and compared. In Section 6 the method used to calculate muon isodose curves in a laminated shield around a high-energy proton accelerator target is described. Results are presented for a shield containing an air gap and for the same shield with the air gap omitted for the case of 500-GeV protons incident on a beryllium target.

2. TRANSPORT EQUATION FOR A ZERO-WIDTH MUON BEAM NORMALLY INCIDENT ON A LAMINATED SLAB SHIELD

The approximate muon transport equation to be used is of the Fermi-Eyges[4,6] type and can be derived from the energy-integrated Boltzmann equation assuming small-angle elastic and nonelastic scattering. The zero-width beam of muons is assumed to be monoenergetic, with kinetic energy E_μ, and incident in the z_μ direction on a series of laminated slabs of different materials. The particles are deflected laterally in the x_μ and y_μ directions by small-angle multiple scattering, giving them a spatial and angular distribution. A model of continuous slowing down along a fictitious straight-line trajectory in the direction of the incident beam determines a slowing-down energy, $E_S(E_\mu,z_\mu)$. This is used as the average energy for all muons at any position, $\vec{R}(x_\mu,y_\mu,z_\mu)$, in a

given z_μ plane. In effect, the cross sections for all collisions occurring in this plane are evaluated at the same initial energy, E_S.

For the particular case of a slab that is either a vacuum or a low-density air gap in which slowing down and multiple scattering can be neglected, the Boltzmann equation indicates the flux is a constant along any straight-line trajectory in the direction of the momentum. (Muon decay is neglected.) The Eyges approximate solution for the lateral and angular flux distribution satisfies this condition. This means that the coefficient for the "width" of the angular distribution is unchanged by the streaming through a vacuum, and the coefficient for the "width" of the lateral distribution correctly takes it into account.

The Boltzmann equation for the energy and angle-dependent muon flux $\Phi(\vec{R},E,\vec{\Omega})$, neglecting decay, can be written in the form:

$$\vec{\Omega}\cdot\vec{\nabla}\Phi(\vec{R},E,\vec{\Omega}) = S_{coll}(\vec{R},E,\vec{\Omega}) + S_o(E_\mu,\vec{\Omega}_\mu)\ \delta(\vec{\Omega}-\vec{\Omega}_\mu)\ \delta(E-E_\mu)\ \delta(\vec{R})\ , \tag{2.1}$$

$$S_{coll}(\vec{R},E,\vec{\Omega}) = \int_E^{E_\mu} dE' \int d\vec{\Omega}'\ \Phi(\vec{R},E',\vec{\Omega}')\ \frac{d^2\Sigma(E',E,\vec{\Omega}'\cdot\vec{\Omega},\vec{R})}{dEd\Omega}$$

$$- \Sigma(E,\vec{R})\ \Phi(\vec{R},E,\vec{\Omega})\ , \tag{2.2}$$

$$S_{coll}(\vec{R},E,\vec{\Omega}) = M(\vec{R},E,\vec{\Omega}) + \frac{\partial q(\vec{R},E,\vec{\Omega})}{\partial E} \tag{2.3}$$

$$M(\vec{R},E,\vec{\Omega}) = \sum_{\nu=C,B,N,P} M_\nu(\vec{R},E,\vec{\Omega})\ , \tag{2.4}$$

$$q(\vec{R},E,\vec{\Omega}) = \sum_{\nu=I,B,N,P} q_\nu(\vec{R},E,\vec{\Omega})\ , \tag{2.5}$$

$$M_\nu(\vec{R},E,\vec{\Omega}) = \int_E^{E_\mu} dE' \int d\vec{\Omega}'[\Phi(\vec{R},E',\vec{\Omega}') - \Phi(\vec{R},E',\vec{\Omega})]\ \frac{d^2\Sigma_\nu(E',E,\vec{\Omega}'\cdot\vec{\Omega},\vec{R})}{dEd\Omega}\ , \tag{2.6}$$

$$q_\nu(\vec{R},E,\vec{\Omega}) = \int_E^{E_\mu} dE'\ \Phi(\vec{R},E',\vec{\Omega}) \int_o^E dE''\ \frac{d\Sigma_\nu(E',E'',\vec{R})}{dE''}\ , \tag{2.7}$$

where

$\vec{R}$ = the position vector of the muon, measured from the point of incidence of the muon beam on the shield,

E = the kinetic energy of the muon,

E_μ = the initial kinetic energy of the muon beam,

$\vec{\Omega}$ = a unit vector in the direction of the momentum,

$\vec{\Omega}_\mu$ = a unit vector in the incident beam direction,

$\Phi(\vec{R},E,\vec{\Omega})$ = the number of muons per unit kinetic energy and solid angle per cm^2 per sec in the direction $\vec{\Omega}$; the dependence on E_μ and $\vec{\Omega}_\mu$ is suppressed,

$S_o(E_\mu,\vec{\Omega}_\mu)dE_\mu d\vec{\Omega}_\mu$ = the number of muons per sec in $dE_\mu d\vec{\Omega}_\mu$ in the incident beam,

ν = an index indicating the type of scattering process,

= I,C,B,N,P for atomic ionization and excitation (assumed straightahead), Coulomb scattering (assumed elastic), bremsstrahlung production, nonelastic nuclear scattering, and electron pair production, respectively.

If

$n_j(\vec{R}) = n_j(z_\mu)$ = the number of atoms of type j per cm^3 at $\vec{R}$ (or z_μ in slab geometry),

$\dfrac{d^2\sigma_{j\nu}(E',E,\cos\theta)}{dEd\Omega}$ = the differential scattering cross section per unit kinetic energy and solid angle for scattering by process ν and atom of type j from E' to E through angle θ,

and

$$\cos\theta = \vec{\Omega}'\cdot\vec{\Omega} ,$$

then

$$\frac{d^2\Sigma_\nu(E',E,\vec{\Omega}'\cdot\vec{\Omega},\vec{R})}{dEd\Omega} = \sum_j n_j(\vec{R}) \frac{d^2\sigma_{j\nu}(E',E,\cos\theta)}{dEd\Omega} , \qquad (2.8)$$

$$\frac{d\Sigma_\nu(E',E,\vec{R})}{dE} = \int d\vec{\Omega}' \frac{d^2\Sigma_\nu(E',E,\vec{\Omega}'\cdot\vec{\Omega},\vec{R})}{dEd\Omega} , \tag{2.9}$$

$$\Sigma_\nu(E,\vec{R}) = \int_0^E dE'' \frac{d\Sigma_\nu(E,E'',\vec{R})}{dE''} , \tag{2.10}$$

$$\Sigma(E,\vec{R}) = \sum_{\nu=I,C,B,N,P} \Sigma_\nu(E,\vec{R}) , \tag{2.11}$$

$$\frac{d^2\Sigma(E',E,\vec{R})}{dEd\Omega} = \sum_{\nu=I,C,B,N,P} \frac{d^2\Sigma_\nu(E',E,\vec{R})}{dEd\Omega} \tag{2.12}$$

In Eq. (2.3),

$q(\vec{R},E,\vec{\Omega})$ = the muon slowing-down density past E in the straightahead approximation for all processes; it is zero for elastic collisions, so Coulomb scattering is not included;

$M(\vec{R},E,\vec{\Omega})dEd\vec{\Omega}$ = the difference in production rate in dE about E from muons scattered into, and out of, $d\vec{\Omega}$ about $\vec{\Omega}$ per unit time and volume.

The function $M(\vec{R},E,\vec{\Omega})$ is zero if the scattering cross sections are all straightahead; in particular, the atomic ionization and excitation cross section is assumed not to contribute to M, although it makes the major contribution to q.

The basic concept of what follows is, first, to expand the integrand of $M(\vec{R},E,\vec{\Omega})$ in the usual small-angle Taylor series, and second, to determine the average or mean energy of the muons by putting M = 0 and replacing $\partial q/\partial E$ by continuous slowing down along $\vec{\Omega}_\mu$.

Following the usual methods for the small-angle multiple-scattering approximation[4,7], the flux $\Phi(\vec{R},E',\vec{\Omega}')$ in $M_\nu(\vec{R},E,\vec{\Omega})$, Eq. (2.6), can be expanded about $\Phi(\vec{R},E',\vec{\Omega})$ in a Taylor series in the variables:

$$\Omega'_x = \sin\theta \cos\phi \ ; \quad \Omega'_y = \sin\theta \sin\phi \quad , \tag{2.13}$$

if

θ = the scattering angle and the polar angle of $\vec{\Omega}'$ with respect to $\vec{\Omega}$,

ϕ = the azimuthal angle of $\vec{\Omega}'$ about $\vec{\Omega}$.

Let

θ_P = the polar angle of $\vec{\Omega}$ with respect to $\vec{\Omega}_\mu$,

ϕ_P = the azimuthal angle of $\vec{\Omega}$ about $\vec{\Omega}_\mu$,

then

$$u = \tan\theta_P \cos\phi_P \; ; \quad v = \tan\theta_P \sin\phi_P$$
$$\omega = \vec{\Omega}\cdot\vec{\Omega}_\mu = \cos\theta_P = \frac{1}{\sqrt{1+u^2+v^2}} \quad , \tag{2.14}$$

$$\nabla^2_\Omega = \frac{\partial^2}{\partial\theta_P^2} + \frac{1}{\tan\theta_P}\frac{\partial}{\partial\theta_P} + \frac{1}{\sin^2\theta_P}\frac{\partial^2}{\partial\phi_P^2} \quad , \tag{2.15}$$

$$= \frac{1}{\omega^2}\left\{(1+u^2)\frac{\partial^2}{\partial u^2} + (1+v^2)\frac{\partial^2}{\partial v^2} + 2uv\frac{\partial^2}{\partial u\partial v} + 2u\frac{\partial}{\partial u} + 2v\frac{\partial}{\partial v}\right\}$$

$$\rightarrow \frac{\partial^2}{\partial u^2} + \frac{\partial^2}{\partial v^2} \tag{2.16}$$

for small u and v.

The first nonvanishing terms in $M_\nu(\vec{R},E,\vec{\Omega})$ are then

$$M_\nu(\vec{R},E,\vec{\Omega}) = \int_E^{E_\mu} dE' \int_0^{2\pi} d\phi \int_0^{\pi} d\theta \, \sin\theta \, \frac{d^2\Sigma_\nu}{dEd\Omega}(E',E,\cos\theta,\vec{R}) \, \frac{\sin^2\theta}{4}$$

$$\times \left[\frac{\partial^2\Phi(\vec{R},E',\vec{\Omega}')}{\partial\Omega_x'^2} + \frac{\partial^2\Phi(\vec{R},E',\vec{\Omega}')}{\partial\Omega_y'^2}\right]_{\substack{\Omega_x'=0\\ \Omega_y'=0}} \quad , \tag{2.17}$$

$$= \nabla^2_\Omega \int_E^{E_\mu} dE' \; \Phi(\vec{R},E',\vec{\Omega}) \, \frac{d\chi_\nu^2(E',E,\vec{R})}{dE} \quad , \tag{2.18}$$

where the term in square brackets in Eq. (2.17) equals $\nabla^2_\Omega \, \Phi(\vec{R},E',\vec{\Omega})$, and

$$\frac{d\chi_\nu^2(E',E,\vec{R})}{dE} = \int_0^{2\pi} d\phi \int_0^{\pi} d\theta \, \frac{\sin^3\theta}{4} \, \frac{d^2\Sigma_\nu(E',E,\cos\theta,\vec{R})}{dEd\Omega} \quad , \tag{2.19}$$

$$\frac{d\chi^2(E',E,\vec{R})}{dE} = \sum_{\nu=C,B,N,P} \frac{d\chi_\nu^2(E',E,\vec{R})}{dE} \quad . \tag{2.20}$$

Define also

$$\chi_\nu^2(E,\vec{R}) = \int_0^E dE'' \frac{d\chi_\nu^2(E,E'',\vec{R})}{dE''} , \tag{2.21}$$

$$\chi^2(E,\vec{R}) = \sum_{\nu=C,B,N,P} \chi_\nu^2(E,\vec{R}) . \tag{2.22}$$

= one-fourth the total mean-square scattering angle per unit distance.

The Boltzmann equation for the energy-dependent muon flux is then

$$\vec{\Omega}\cdot\vec{\nabla}\Phi(\vec{R},E,\vec{\Omega}) = \frac{\partial q(\vec{R},E,\vec{\Omega})}{\partial E} + S_o(E_\mu,\vec{\Omega}_\mu)\ \delta(\vec{\Omega}-\vec{\Omega}_\mu)\ \delta(E-E_\mu)\ \delta(\vec{R})$$

$$+ \nabla_\Omega^2\ \chi_C^2(E,\vec{R})\ \Phi(\vec{R},E,\vec{\Omega})$$

$$+ \nabla_\Omega^2 \int_E^{E_\mu} dE'\ \Phi(\vec{R},E',\vec{\Omega}) \sum_{\nu=B,N,P} \frac{d\chi_\nu^2(E',E,\vec{R})}{dE} \tag{2.23}$$

in the small-angle multiple-scattering approximation, where the $\delta(E'-E)$ factor in the elastic Coulomb scattering cross section has been integrated over explicitly. Integrating over all energies,

$$\psi(\vec{R},\vec{\Omega}) = \int_0^{E_\mu+\varepsilon} dE\ \Phi(\vec{R},E,\vec{\Omega}) \qquad \varepsilon << 0 , \tag{2.24}$$

$$\int_0^{E_\mu+\varepsilon} \frac{\partial q}{\partial E} = q(\vec{R},E_\mu+\varepsilon,\vec{\Omega}) - q(\vec{R},0,\vec{\Omega}) = 0 , \tag{2.25}$$

$$\vec{\Omega}\cdot\vec{\nabla}\psi(\vec{R},\vec{\Omega}) = S_o(E_\mu,\vec{\Omega}_\mu)\ \delta(\vec{\Omega}-\vec{\Omega}_\mu)\ \delta(\vec{R})$$

$$+ \int_0^{E_\mu+\varepsilon} \chi^2(E',\vec{R})\ \nabla_\Omega^2\Phi(\vec{R},E',\vec{\Omega})\ dE' , \tag{2.26}$$

where the integrations over E and E' have been interchanged and Eqs. (2.20) to (2.22) have been used. The function $\chi^2(E',\vec{R})$ is removed from under the integral sign by evaluating the initial energy E' at a mean value, E_m; E_m is a function of $(\vec{R},\vec{\Omega},E_\mu,\vec{\Omega}_\mu)$ in general, but a knowledge of this

functional dependence would involve the solution of Eq. (2.23) and would not lead to the Eyges equation anyway. Equation (2.26) becomes

$$\vec{\Omega}\cdot\vec{\nabla}\psi(\vec{R},\vec{\Omega}) = S_o(E_\mu,\vec{\Omega}_\mu)\ \delta(\vec{\Omega}-\vec{\Omega}_\mu)\ \delta(\vec{R}) + \chi^2(E_m,\vec{R})\ \nabla^2_\Omega\psi(\vec{R},\vec{\Omega})\ . \tag{2.27}$$

For slab geometry,

$$\chi^2(E_m,\vec{R}) = \chi^2(E_m,z_\mu)\ .$$

Let z_1, z_2, $z_3,\ldots z_{n-1}\ldots$be the positions of successive interfaces in the direction $\vec{\Omega}_\mu$. In the straightahead continuous slowing-down approximation, $\chi^2 = 0$, and in Eq. (2.23),

$$\frac{\partial q(\vec{R},E,\vec{\Omega})}{\partial E} \longrightarrow \rho_n(z_\mu)\ \frac{\partial}{\partial E}\left[S_n(E)\ \Phi(\vec{R},E,\vec{\Omega})\right] \tag{2.28}$$

in slab n,

$\rho_n(z_\mu)$ = the density in g/cm^3 in slab n,

$$S_n(E) = \sum_{\nu=I,B,N,P} S_{n\nu}(E)\ , \tag{2.29}$$

$S_{n\nu}(E)$ = the energy loss per unit distance in MeV/g/cm^2 for process ν, in slab n. The energy-dependent flux is then

$$\Phi(\vec{R},E,\vec{\Omega}) = S_o(E_\mu,\vec{\Omega}_\mu)\ \delta(\vec{\Omega}-\vec{\Omega}_\mu)\ \delta(x_\mu)\ \delta(y_\mu)\ \delta[E-E_S(E_\mu,z_\mu)]\ . \tag{2.30}$$

The slowing-down energy, $E_S(E_\mu,z_\mu)$, is defined by the set of equations:

$$\begin{aligned}
\int_{E_1}^{E_\mu} \frac{dE'}{S_1(E')} &= \int_o^{z_1} dz'\ \rho_1(z') \\
\int_{E_2}^{E_1} \frac{dE'}{S_2(E')} &= \int_{z_1}^{z_2} dz'\ \rho_2(z') \\
&\vdots \\
\int_{E_{S(E_\mu,z_\mu)}}^{E_{n-1}} \frac{dE'}{S_n(E')} &= \int_{z_{n-1}}^{z_\mu} dz'\ \rho_n(z')
\end{aligned}\ , \tag{2.31}$$

if z_μ is in slab n and is less than the range of the muon of initial energy E_μ. The energies E_1, E_2, E_3,...E_{n-1}... are the slowing-down energies at each successive interface.

The Eyges equation is obtained from Eq. (2.27) if E_m is replaced by $E_S(E_\mu,z_\mu)$ and if small u and v; i.e., small angular deflections from the direction $\vec{\Omega}_\mu$, are assumed. Then

$$\left\{ \frac{\partial}{\partial z_\mu} + u \frac{\partial}{\partial x_\mu} + v \frac{\partial}{\partial y_\mu} - \chi^2[E_S(E_\mu,z_\mu),z_\mu]\left(\frac{\partial^2}{\partial u^2} + \frac{\partial^2}{\partial v^2}\right)\right\} \psi(z_\mu,x_\mu,y_\mu,u,v)$$

$$= S_o(E_\mu,\vec{\Omega}_\mu)\ \delta(u)\ \delta(v)\ \delta(x_\mu)\ \delta(y_\mu)\ \delta(z_\mu)\ . \qquad (2.32)$$

Note that $E_S(E_\mu,z_\mu)$ is continuous across the interfaces, but χ^2 may be a discontinuous function of z_μ if the scattering cross sections and the density change discontinuously from one material to another.

The Eyges solution is:

$$\psi(\vec{R},\vec{\Omega}) = S_o(E_\mu,\vec{\Omega}_\mu)\ \frac{\exp[-\frac{N}{4B}]}{(4\pi)^2\ B}\ , \qquad (2.33)$$

$$N(\vec{R},\vec{\Omega},E_\mu,\vec{\Omega}_\mu) = A_2(u^2+v^2) - 2A_1(ux_\mu + vy_\mu) + A_o(x_\mu^2+y_\mu^2)\ , \qquad (2.34)$$

$$A_o = \int_o^{z_\mu} dz'_\mu\ \chi^2[E_S(E_\mu,z'_\mu),z'_\mu]\ , \qquad (2.35)$$

$$A_1 = \int_o^{z_\mu} dz'_\mu\ \chi^2[E_S(E_\mu,z'_\mu),z'_\mu](z_\mu - z'_\mu)\ , \qquad (2.36)$$

$$A_2 = \int_o^{z_\mu} dz'_\mu\ \chi^2[E_S(E_\mu,z'_\mu),z'_\mu](z_\mu - z'_\mu)^2\ , \qquad (2.37)$$

$$B = A_o\ A_2 - A_1^2 = B(E_\mu,z_\mu)\ . \qquad (2.38)$$

Consider the case of a vacuum gap beginning at z_n and ending at z_{n+1}. The quantity $\chi^2(E_S,z_\mu)$ is zero in the vacuum, and for $z_n \leq z_\mu \leq z_{n+1}$

$$E_S(E_\mu, z_\mu) = E_S(E_\mu, z_n) = E_n \ , \tag{2.39}$$

$$A_o(E_\mu, z_\mu) = A_o(E_\mu, z_n) \ , \tag{2.40}$$

$$A_1(E_\mu, z_\mu) = A_1(E_\mu, z_n) + (z_\mu - z_n)\, A_o(E_\mu, z_n) \ , \tag{2.41}$$

$$A_2(E_\mu, z_\mu) = A_2(E_\mu, z_n) + 2(z_\mu - z_n)\, A_1(E_\mu, z_n) + (z_\mu - z_n)^2\, A_o(E_\mu, z_n) \ . \tag{2.42}$$

If $\vec{R}(x_\mu, y_\mu, z_\mu)$ and $\vec{R}_n(x_n, y_n, z_n)$ are points on a straight-line trajectory along $\vec{\Omega}$, so that

$$\begin{aligned} \vec{R} &= \vec{R}_n + \ell\vec{\Omega} \ , \\ z_\mu &= \vec{R}\cdot\vec{\Omega}_\mu = z_n + \ell\omega \ , \\ x_\mu &= x_n + \ell\omega u = x_n + (z_\mu - z_n)u \ , \\ y_\mu &= y_n + \ell\omega v = y_n + (z_\mu - z_n)v \ , \end{aligned} \tag{2.43}$$

it is easy to show by substitution into Eq. (2.34), using Eqs. (2.40) to (2.43), that

$$N(\vec{R}, \vec{\Omega}, E_\mu, \vec{\Omega}_\mu) = N(\vec{R}_n, \vec{\Omega}, E_\mu, \vec{\Omega}_\mu) \ , \tag{2.44}$$

$$B(E_\mu, z_\mu) = B(E_\mu, z_n) \ . \tag{2.45}$$

Then

$$\psi(\vec{R}, \vec{\Omega}) = \psi(\vec{R}_n, \vec{\Omega}) \ ; \tag{2.46}$$

i.e., the energy-integrated angular flux in the Eyges approximation is constant along straight-line trajectories in a vacuum, as expected.

Integration of Eq. (2.33) over all x_μ and y_μ gives

$$\psi(z_\mu, \vec{\Omega}) = \frac{S_o(E_\mu, \vec{\Omega}_\mu)}{4\pi\, A_o} \exp\left[-\frac{(u^2 + v^2)}{4A_o}\right] = \psi(z_n, \vec{\Omega}) \tag{2.47}$$

for the angular distribution at z_μ; ψ is unaffected by streaming through

the vacuum because the coefficient $A_o(E_\mu, z_\mu)$ is equal to $A_o(E_\mu, z_n)$ if z_μ lies in the vacuum. However, the coefficients A_1 and A_2 are increased by the streaming, as shown by Eqs. (2.41) and (2.42). The change in A_2 for E_μ equal to 500 GeV and 200 GeV in an air gap of 70 m in width is shown in Section 4, Fig. 4; multiple scattering and slowing down in air are included in these computations of A_2.

3. ENERGY LOSS AND DIFFERENTIAL CROSS-SECTION DATA

3.1 Energy loss per unit distance

The energy loss of charged particles due to the ionization and excitation of atomic electrons is well established and may be computed from the Bethe-Block[8] formula with the density-effect correction given by Sternheimer[9-12]. For some materials that contain a mixture of elements (soil in this paper), the density-effect correction is not available and is computed using the asymptotic form of the correction[13].

The energy loss of muons due to bremsstrahlung production, pair production, and nonelastic nuclear collisions has been considered in detail by Hayman *et al.*[5], by Kobayakawa[14], and, using the results of Hayman *et al.*, by Thomas[15]. In the work reported here, the recommendations of Hayman *et al.* have been used for the energy loss due to bremsstrahlung and pair production, and the recommendations of Kobayakawa have been used for the energy loss due to nonelastic nuclear interactions.

Calculations have been carried out for shields of iron and of soil, and of an iron-air-soil combination. The soil was assumed to be composed of 58.3% oxygen, 32.7% aluminum, 6.1% calcium, and 2.9% iron. The density of iron was taken to be 7.8 g/cm^3, that of soil, 2.0 g/cm^3, and that of air, 1.29×10^{-3} g/cm^3.

The muon stopping power S, as well as the individual contributions to the stopping power, S_ν's, is shown in Fig. 1 as a function of muon energy for iron and soil. The values of S_N for iron and soil are the same because of the assumptions made by Kobayakawa[14].

3.2 Muon-nucleus elastic Coulomb collisions

The differential cross section for the elastic Coulomb scattering of a muon by a nucleus may be written[6,16-19]

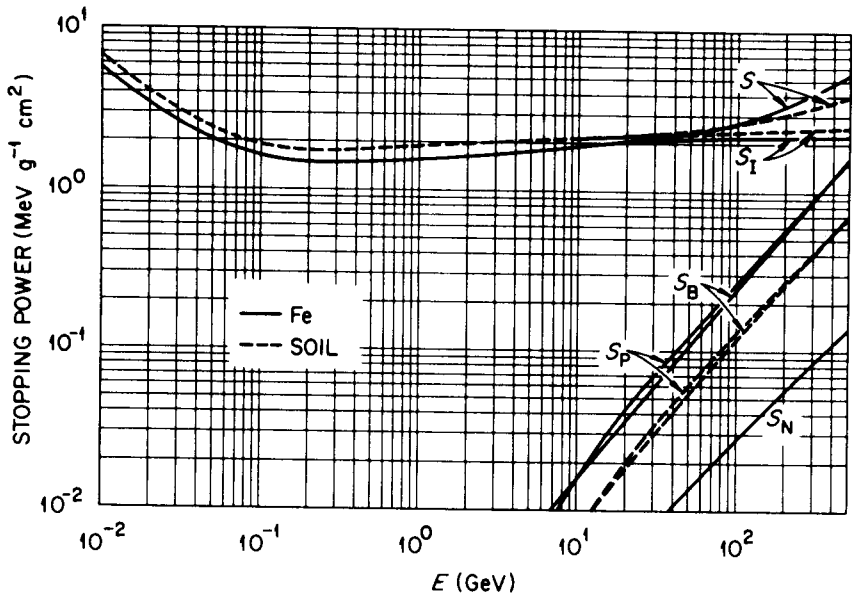

Fig. 1 Stopping power of iron and soil for muons vs muon energy. Also shown are the contributions from the various physical processes considered in calculating the total stopping power.

$$\frac{d\sigma_{jC}}{d\Omega} = Z_j(Z_j+1)\,\frac{e^4}{P'^2\beta^2}\,\frac{[F_j(\kappa)]^2}{[1-\cos\theta-\frac{1}{2}\theta_s^2]^2}\,R(\varepsilon',\theta)\ , \tag{3.1}$$

$$F_j(\kappa) = \frac{\int_0^\infty \rho_{Nj}(r)\,\frac{\sin\kappa r}{\kappa r}\,r^2dr}{\int_0^\infty \rho_{Nj}(r)\,r^2dr}\ , \tag{3.2}$$

$$\kappa^2 = \hbar^{-2}\ 2P'^2(1-\cos\theta)\ , \tag{3.3}$$

$$\beta = \frac{P'}{\varepsilon'}\ , \tag{3.4}$$

$$\theta_s^2 = \left[\frac{Z_j^{1/3}\,\alpha\,m_e}{0.885}\right]^2 \frac{1}{P'^2}\left[1.13 + 3.76\left(\frac{Z_j\alpha}{\beta}\right)^2\right]\ , \tag{3.5}$$

where

Z_j = the atomic number of the jth element,

e = the electronic charge,

P', ε' = the momentum and total energy of the incident muon,

θ = the scattering angle,

θ_s = a correction to the cross section to take into account the screening of the nucleus by the atomic electrons[6,18],

$F_j(\kappa)$ = the nuclear form factor[19],

$\rho_{Nj}(r)$ = the charge distribution of the jth nucleus,

$R(\varepsilon',\theta)$ = the ratio of Mott-to-Rutherford scattering[16,17],

$\hbar$ = Planck's constant divided by 2π,

α = the fine structure constant,

m_e = the electronic mass.

To evaluate the form factor, a trapezoidal charge distribution of the form[19]

$$\begin{aligned} \rho_{Nj}(r) &= D_{3j} && 0 \leq r \leq C_j - D_3 \\ &= D_{3j}\frac{(C_j+D_3-r)}{2D_3} && C_j - D_3 < r \leq C_j + D_3 \\ &= 0 && r > C_j + D_3 \quad , \end{aligned} \tag{3.6}$$

where

$C_j = 1.07 \times 10^{-13}\ A_j^{1/3}$ cm

$D_3 = 1.50 \times 10^{-13}$ cm

A_j = the number of nucleons in the jth nucleus ,

has been used. This charge distribution is in reasonable agreement with the electron-scattering data and at the same time is sufficiently simple that the form factor may be obtained analytically.

With this cross section, the calculation of χ_C^2 from Eq. (3.1) is straightforward, but since $R(\varepsilon,\theta)$ is given in the form of an infinite series, the numerical computations are quite lengthy. On the other hand, the quantity $R(\varepsilon,\theta)$ is not appreciably different from unity at the energies of interest here, and therefore the approximation $R(\varepsilon,\theta) = 1$ is quite satisfactory.

In Table 1 the quantity χ_C^2, calculated with $R(\varepsilon,\theta)$ and calculated in the approximation $R(\varepsilon,\theta) = 1$, is shown as a function of energy for iron and soil. It may be seen from the values in the table that the approximation $R(\varepsilon,\theta) = 1$ is very good over the energy range 0.01 to 500 GeV, and therefore this approximation will be used in the calculations reported here.

Table 1

One-fourth the mean-square scattering angle per unit distance from Coulomb scattering vs energy

Energy (GeV)	χ_C^2 For Iron (1/cm)		
	$R \neq 1$	$R = 1$	Eq. (3.7)
0.01	1.57×10^{-1}	1.55×10^{-1}	1.71×10^{-1}
0.05	8.71×10^{-3}	8.61×10^{-3}	8.89×10^{-3}
0.1	2.70×10^{-3}	2.67×10^{-3}	2.73×10^{-3}
0.5	1.79×10^{-4}	1.78×10^{-4}	1.82×10^{-4}
1.0	5.14×10^{-5}	5.13×10^{-5}	5.22×10^{-5}
5.0	2.36×10^{-6}	2.36×10^{-6}	2.41×10^{-6}
10.0	6.03×10^{-7}	6.03×10^{-7}	6.14×10^{-7}
50.0	2.45×10^{-8}	2.45×10^{-8}	2.50×10^{-8}
100.0	6.14×10^{-9}	6.14×10^{-9}	6.25×10^{-9}
200.0	1.54×10^{-9}	1.54×10^{-9}	1.56×10^{-9}
300.0	6.84×10^{-10}	6.84×10^{-10}	6.96×10^{-10}
400.0	3.84×10^{-10}	3.84×10^{-10}	3.91×10^{-10}
500.0	2.46×10^{-10}	2.46×10^{-10}	2.51×10^{-10}

Table 1 (cont'd.)

One-fourth the mean-square scattering angle per unit distance from Coulomb scattering vs energy

Energy (GeV)	χ_C^2 For Soil (1/cm)		
	$R \neq 1$	$R = 1$	Eq. (3.7)
0.01	1.98×10^{-2}	1.98×10^{-2}	2.19×10^{-2}
0.05	1.09×10^{-3}	1.09×10^{-3}	1.14×10^{-3}
0.1	3.40×10^{-4}	3.39×10^{-4}	3.50×10^{-4}
0.5	2.27×10^{-5}	2.26×10^{-5}	2.33×10^{-5}
1.0	6.52×10^{-6}	6.51×10^{-6}	6.68×10^{-6}
5.0	3.00×10^{-7}	3.00×10^{-7}	3.08×10^{-7}
10.0	7.65×10^{-8}	7.65×10^{-8}	7.86×10^{-8}
50.0	3.11×10^{-9}	3.11×10^{-9}	3.20×10^{-9}
100.0	7.80×10^{-10}	7.80×10^{-10}	8.00×10^{-10}
200.0	1.95×10^{-10}	1.95×10^{-10}	2.00×10^{-10}
300.0	8.67×10^{-11}	8.67×10^{-11}	8.91×10^{-11}
400.0	4.88×10^{-11}	4.88×10^{-11}	5.01×10^{-11}
500.0	3.13×10^{-11}	3.13×10^{-11}	3.21×10^{-11}

In the previous muon shielding calculations[2,3], the approximate expression

$$\chi_C^2(E') = \left[\frac{E_s}{2\beta P'}\right]^2 \frac{1}{x_o} , \tag{3.7}$$

$$E_s = \left[\frac{4\pi}{\alpha}\right]^{\frac{1}{2}} m_e$$

$$\frac{1}{x_o} = \sum_j \left[n_j Z_j(Z_j+1)\, 4\alpha r_o^2 \log(183\, Z_j^{-1/3})\right] ,$$

where

r_o = the classical electron radius,

has been used. In the last column of Table 1, this quantity is given as a function of muon energy for iron and soil, respectively. It can be seen that the values of χ_C^2 given by Eq. (3.7) are slightly larger than those obtained with the cross section given by Eq. (3.1) with either $R = 1$ or $R \neq 1$.

3.3 Bremsstrahlung production from muon-nucleus collisions

The cross-section differential in final electron energy and angle when an electron radiates in the field of a nucleus has been given by McCormick *et al.*[20]. This cross section, however, was derived for a point nucleus and cannot be applied directly to the high-energy muons of interest here because the corrections due to the nuclear charge distribution are not negligible. A cross-section differential in photon energy and in the angles of the final electron and photon when an electron radiates in the field of a nucleus with an arbitrary charge distribution has been given by Biel and Burhop[21]. This cross section can be applied to the muons of interest here, but because the nuclear form factor that enters into the cross section depends on the angles of both the final muon and the photon, the integrations to obtain the cross section that is differential only in final muon energy and angle are problematic. To avoid this complication, an approximate nuclear form-factor correction has been made. To understand the approximation that is used, note that the nuclear form factor that enters into the cross section given by Biel and Burhop is the same as that given by Eq. (3.2) but with κ^2 given by

$$\kappa^2 = (\hbar)^{-2} \, |\vec{P}' - \vec{P} - \vec{K}|^2 \quad , \qquad K = \varepsilon' - \varepsilon \tag{3.8}$$

where

$\vec{P}', \varepsilon'$ = the momentum and total energy of the incident muon,

$\vec{P}, \varepsilon$ = the momentum and total energy of the final muon,

$\vec{K}$ = the photon momentum.

The form factor depends on the emission angles of the photon through κ^2 which may be written

$$\kappa^2 = (\hbar)^{-2} \, [P'^2 - 2\,\vec{P}'\cdot\vec{P} - 2\,\vec{P}'\cdot\vec{K} + P^2 + 2\,\vec{P}\cdot\vec{K} + K^2] \; . \tag{3.9}$$

The approximation that is used here is to assume that the photon is emitted in the direction of the incident muon; i.e., it is assumed that the form factor may be evaluated by taking $\vec{K}$ to be parallel to $\vec{P}'$. When this is done,

$$\kappa^2 = (\hbar)^{-2} \left[P'^2 - 2\, P'\, P \cos\theta - 2\, P'\, K + P^2 + 2\, P\, K \cos\theta + K^2\right] , \qquad (3.10)$$

where

θ = the angle between the initial and final muon momentum.

In this approximation, the form factor is independent of the emission angles of the photon, and the integration over these angles may be carried out as in the case of a point nucleus, so

$$\frac{d^2\sigma_j}{dE d\Omega} = [F_j(\kappa)]^2 \left[\frac{d^2\sigma_j}{dE d\Omega}\right]_P , \qquad (3.11)$$

where

$\frac{d^2\sigma_j}{dE d\Omega}$ = the cross section differential in final muon energy and angle when a muon radiates in the field of a nucleus of type j that has a charge distribution of $\rho_{Nj}(r)$,

$\left[\frac{d^2\sigma_j}{dE d\Omega}\right]_P$ = the cross-section differential in final muon energy and angle when a muon radiates in the field of a point nucleus of type j,

and it is to be understood that the approximate expression for κ, Eq. (3.10), is to be used.

The differential cross section from a point nucleus may be taken from the work of McCormick *et al.*[20]. This cross section, however, was obtained using the Born approximation and is therefore not accurate for high-energy photon emission[22,23]. To correct the cross section in the high frequency limit, it has been multiplied by the factor

$$\frac{2\pi\, Z_j\, \alpha\, \frac{\varepsilon}{P}}{1 - \exp[-2\pi\, Z_j\, \alpha\, \frac{\varepsilon}{P}]} , \qquad (3.12)$$

where the symbols have the same meaning as before. This factor assures

that the differential cross section integrated over all angles of the emitted muon has the correct limit as the muon energy loss approaches the incident muon energy, but since it is not a function of the muon emission angle, it does not give the correct limit as a function of angle, and is therefore only a very approximate correction.

The cross section given by McCormick *et al.*[20] is not corrected for electron screening, and no attempt has been made here to introduce a correction for this effect. The factor of Z_j^2 in the cross section given by McCormick *et al.*, however, has been replaced in the usual manner by $Z_j(Z_j+1)$ to account very approximately for the bremsstrahlung production from atomic electrons[23]. The final form of the bremsstrahlung cross section that is used is then

$$\frac{d^2\sigma_{jB}}{dEd\Omega} = Z_j(Z_j+1)\,[F_j(\kappa)]^2 \frac{2\pi\, Z_j\, \alpha\, \frac{\varepsilon}{P}}{1-\exp[-2\pi\, Z_j\, \alpha\, \frac{\varepsilon}{P}]} \left[\frac{1}{Z_j^2}\frac{d^2\sigma_j}{dEd\Omega}\right]_P , \qquad (3.13)$$

where the cross section for a point nucleus is taken from Ref. 20, and the nuclear charge distribution given in Eq. (3.6) has been used to evaluate the form factor.

The calculation of χ_B^2 is not straightforward because the differential cross section for bremsstrahlung production diverges for small energy losses of the muon, i.e., for the emission of soft photons. This well-known infrared divergence is unphysical and is related to the fact that very soft photon emission is not experimentally distinguishable from elastic scattering[24]. Here the divergence is removed by assuming that the differential cross section may be set equal to zero when the energy loss of a muon with kinetic energy E' is less than $\eta_B E'$ where η_B is a parameter that is to be specified. With this provision, χ_B^2 may be written

$$\chi_B^2(E') = \sum_j 2\pi\, n_j \int_0^{E'(1-\eta_B)} dE \int_{-1}^{1} d(\cos\theta)$$

$$\frac{d^2\sigma_{jB}(E',E,\cos\theta)}{dEd\Omega}\,\frac{\sin^2\theta}{4} \quad . \qquad (3.14)$$

For both iron and soil χ_B^2 is shown in Table 2 as a function of energy for $\eta_B = 10^{-1}$ and $\eta_B = 10^{-4}$. For the range of η_B values considered, χ_B^2 is slowly varying over the energy range 10 to 500 GeV. Furthermore, $\eta_B = 10^{-4}$ means that only 0.01% of the incident muon energy is being neglected, so hopefully the error introduced is not large. In the remainder of the paper, $\eta_B = 10^{-4}$ is used in all calculations.

Table 2

One-fourth the mean-square scattering angle per unit distance from bremsstrahlung production vs energy

Energy (GeV	χ_B^2 For Iron (1/cm)		χ_B^2 For Soil (1/cm)	
	$\eta_B = 10^{-4}$	$\eta_B = 10^{-1}$	$\eta_B = 10^{-4}$	$\eta_B = 10^{-1}$
10	3.29×10^{-9}	2.81×10^{-9}	4.59×10^{-10}	3.95×10^{-10}
50	5.74×10^{-10}	5.54×10^{-10}	8.21×10^{-11}	7.95×10^{-11}
100	2.77×10^{-10}	2.72×10^{-10}	3.99×10^{-11}	3.93×10^{-11}
200	1.35×10^{-10}	1.33×10^{-10}	1.94×10^{-11}	1.93×10^{-11}
300	8.84×10^{-11}	8.79×10^{-11}	1.28×10^{-11}	1.27×10^{-11}
400	6.57×10^{-11}	6.54×10^{-11}	9.49×10^{-12}	9.45×10^{-12}
500	5.23×10^{-11}	5.21×10^{-11}	7.55×10^{-12}	7.52×10^{-12}

3.4 Pair production from muon-nucleus collisions

An approximate cross-section differential in final muon energy and angle when a muon produces an electron-positron pair in the field of a nucleus has been given by Tannenbaum[25].*) This cross section may be written

$$\frac{d^2\sigma_{jP}}{dq^2 dK} = Z_j(Z_j + 1)\,\frac{\alpha^2}{\pi}\,r_o^2\left[\frac{28}{9}\log\frac{2K}{m_e} - \frac{218}{27}\right]$$

$$\left\{\frac{m_e^2}{m_e^2+q^2}\,\frac{1}{q^2}\,\frac{1}{\sqrt{q^2+K^2}}\right\}\left\{1 - \frac{K}{\varepsilon} + \frac{q^2}{4\varepsilon^2} + \frac{K^2}{2\varepsilon^2} - \frac{m_\mu}{\varepsilon^2} - \frac{m_\mu^2 K^2}{q^2\varepsilon^2}\right\}$$

$$q_{min}^2 \le q^2 \le q_{max}^2 \,, \qquad (3.15)$$

*) We thank Dr. Tannenbaum for making this cross section available to us.

where

$$q^2 = (P' - P)^2 = 2[\varepsilon\varepsilon' - m_\mu^2 - |\vec{P}'||\vec{P}| \cos\theta] \ , \tag{3.16}$$

$$q^2_{max} = 2[\varepsilon\varepsilon' - m_\mu^2 + |\vec{P}'||\vec{P}|] \ , \tag{3.17}$$

$$q^2_{min} = 2[\varepsilon\varepsilon' - m_\mu^2 - |\vec{P}'||\vec{P}|] \ , \tag{3.18}$$

$$K = \varepsilon' - \varepsilon \ , \tag{3.19}$$

and the symbols have the same meanings as before. Because of the manner in which it was derived, the cross section given in Eq. (3.15) is invalid at small values of K and, in fact, becomes negative at sufficiently small K. Here it is assumed that the cross section may be set equal to zero for those K values for which the right-hand side of Eq. (3.15) is negative. Then

$$\chi_P^2(E') = \sum_j n_j \int_{K_L}^{\varepsilon'} dK \int_{q^2_{min}}^{q^2_{max}} dq^2 \frac{d^2\sigma_{jP}}{dq^2 dK} \frac{\sin^2\theta}{4} \ , \tag{3.20}$$

$$K_L = \frac{m_e}{2} \exp[\frac{218(9)}{27(28)}] \ ,$$

where $\sin^2\theta$ is to be expressed in terms of q^2 by means of Eq. (3.16). In calculating $\chi_P^2(E')$, the integration over q^2 was carried out analytically and the integration over K was carried out numerically.

3.5 Muon-nucleus nonelastic collisions

The differential cross section for muon-nucleus nonelastic collisions may be written as[14,26]

$$\frac{d^2\sigma_{jN}}{dq^2 dK} = \frac{\alpha}{2\pi} \sigma_j \frac{1}{K|\vec{P}'|^2} \left[\frac{\varepsilon' + (\varepsilon' - K)^2}{q^2} - \frac{2m_\mu^2 K^2}{q^4} - \frac{1}{2}\right]\left[a + (1-a)\left(\frac{\Lambda^2}{q^2+\Lambda^2}\right)^2\right]$$

$$q^2_{min} \le q^2 \le q^2_{max} \ , \ 0 \le K \le K_{max} \ , \tag{3.21}$$

where

$$\begin{aligned} q^2 &= (P' - P)^2 \\ &= 2[\varepsilon'\varepsilon - m_\mu^2 - |\vec{P}'||\vec{P}|\cos\theta] \ , \end{aligned} \tag{3.22}$$

$$q^2_{max} = 2MK \ , \tag{3.23}$$

$$q^2_{min} = 2[\varepsilon'\varepsilon - m_\mu^2 - |\vec{P}'||\vec{P}|] \ , \tag{3.24}$$

$$K = \varepsilon' - \varepsilon \ , \tag{3.25}$$

$$K_{max} = \varepsilon' - \frac{1}{2} M(1 + \frac{m_\mu^2}{M^2}) \ , \tag{3.26}$$

$$\sigma_j = 0.72 \times 10^{-28} \ A_j \ cm^2 \ ,$$

$$\Lambda^2 = 0.365 \ GeV^2 \ ,$$

$$a = 0.1 \ ,$$

M = the nucleon mass,

and the other symbols have the same meanings as before. It should be noted that since σ_j is proportional to A_j, the cross section is independent of atomic weight. The cross section diverges for small K, and therefore, in order to calculate χ_N^2, a cutoff has been introduced in the same manner as in the calculation of χ_B^2. The χ_N^2 is calculated from the equation

$$\chi_N^2(E') = \sum_j n_j \int_{E_{min}}^{E'(1-\eta_N)} dE \int_{q^2_{min}}^{q^2_{max}} dq^2 \frac{d^2\sigma_{jN}}{dq^2 dK} \frac{\sin^2\theta}{4} \tag{3.27}$$

$$E_{min} = \frac{1}{2} M(1 + \frac{m_\mu^2}{M}) - m_\mu \ ,$$

where $\sin^2\theta$ must be expressed in terms of q^2 from Eq. (3.22) and η_N is the cutoff parameter.

Calculated values of χ_N^2 for iron are given in Table 3 for various values of E' and for $\eta_N = 10^{-5}$ and 10^{-11}. The values of χ_N^2 are independent of η_N for this wide range of η_N values. This result is also valid for soil since the cross section is independent of atomic weight. In all subsequent calculations for both iron and soil, $\eta_N = 10^{-11}$ is used.

3.6 The mean-square scattering angle per unit distance*)

In Fig. 2, χ^2, as well as χ_C^2, χ_B^2, χ_P^2, and χ_N^2, is shown as a function of muon energy for iron and soil. Below approximately 10 GeV, χ_B^2, χ_P^2,

*) Note that χ^2 is one-fourth the mean-square scattering angle per unit distance.

Table 3

One-fourth the mean-square scattering angle per unit distance from nonelastic nuclear collisions vs energy

Energy (GeV)	χ_N^2 For Iron (1/cm)	
	$\eta_N = 10^{-5}$	$\eta_N = 10^{-11}$
10	8.30×10^{-9}	8.30×10^{-9}
25	3.44×10^{-9}	3.44×10^{-9}
50	1.87×10^{-9}	1.87×10^{-9}
100	1.04×10^{-9}	1.04×10^{-9}
200	5.75×10^{-10}	5.75×10^{-10}
300	4.07×10^{-10}	4.07×10^{-10}
400	3.18×10^{-10}	3.18×10^{-10}
500	2.59×10^{-10}	2.59×10^{-10}

and χ_N^2 become negligible compared to χ_C^2. At all energies the contribution of χ_P^2 to χ^2 is negligible. The contribution of χ_B^2 to χ^2 is small at all energies, but at the higher energies it is not completely negligible. At the highest energies considered, χ_N^2 becomes comparable to χ_C^2.

It is to be noted that the units of χ^2 used in Fig. 2 is cm^{-1}. An appreciable part of the difference shown in the figure between χ^2 for iron and soil is due to the difference in density between iron and soil.

4. THE LATERAL SPREAD OF A ZERO-WIDTH BEAM OF MONOENERGETIC MUONS NORMALLY INCIDENT ON HOMOGENEOUS AND LAMINATED SLAB SHIELDS

The solution to the muon transport equation for a narrow beam of monoenergetic muons normally incident on a laminated slab shield was presented in Section 2. If one integrates this solution over all angles, the omnidirectional energy-integrated muon flux may be written

$$\psi(E_\mu, z_\mu, r_\mu) = \frac{1}{4\pi\, A_2(E_\mu, z_\mu)} \exp\left[-\frac{r_\mu^2}{4A_2(E_\mu, z_\mu)}\right] \tag{4.1}$$

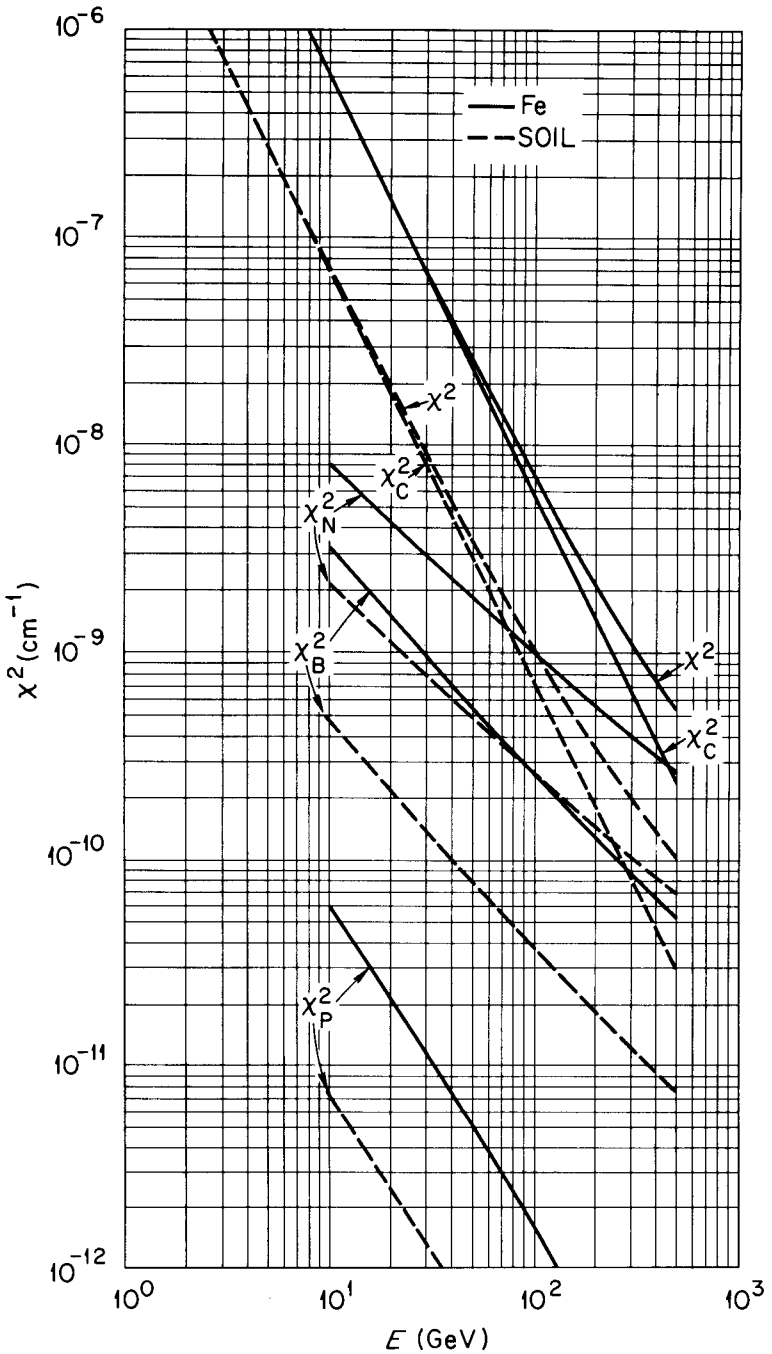

Fig. 2 One-fourth the mean-square scattering angle per unit distance vs muon energy. Also shown are the contributions from the various physical processes considered in calculating the mean-square scattering angle.

$$A_2(E_\mu, z_\mu) = \int_0^{z_\mu} \chi^2[E_S(E_\mu, z'_\mu), z'_\mu]\ (z_\mu - z'_\mu)^2\ dz'_\mu\ , \tag{4.2}$$

$$\begin{aligned} \int_{E_1}^{E_\mu} \frac{dE'}{S_1(E')} &= \rho_1 z_1 \\ \int_{E_2}^{E_1} \frac{dE'}{S_2(E')} &= \rho_2 (z_2 - z_1) \\ &\vdots \\ \int_{E_S}^{E_{n-1}} \frac{dE'}{S_n(E')} &= \rho_n (z'_\mu - z_{n-1}) \end{aligned} \quad , \tag{4.3}$$

where

r_μ = the polar radius vector in planes normal to the z_μ axis,

and, in writing the set of Eqs. (4.3), the density ρ_n has been assumed constant in a subslab. In the case of a homogeneous shield, Eq. (4.1) is unchanged, χ^2 in Eq. (4.2) is a function of E_S only, and the set of Eqs. (4.3) reduces to a single equation.

The quantity $\rho^2 A_2$ is shown in Fig. 3 as a function of shield depth in g/cm^2 for 200-GeV and 500-GeV muons normally incident on shields of iron and soil. In the figure, the solid lines give the results when χ^2 is used in Eq. (4.2) and the dashed lines give the results when χ_C^2 is used for χ^2 in Eq. (4.2), i.e., when only Coulomb scattering is considered. The quantity A_2 has been multiplied by ρ^2 in the figure to remove insofar as possible the density dependence of A_2. There is, nevertheless, considerable difference between $\rho^2 A_2(E_\mu, z_\mu)$ for iron and soil. Since in the approximation that is used here there is a unique relation between particle energy and depth [see Eq. (4.3], the curves in Fig. 3 end at the range of the incident particle. It is to be noted that even when measured in g/cm^2 there is a considerable difference between the range of a 500-GeV muon in iron and in soil. The dashed curves in the figure were obtained using Coulomb scattering only and therefore correspond to the approximation used in the previous calculations[1-3]. As the figure indicates, there is some difference for 200-GeV incident muons and considerable difference for 500-GeV muons between the solid curves that include an estimate

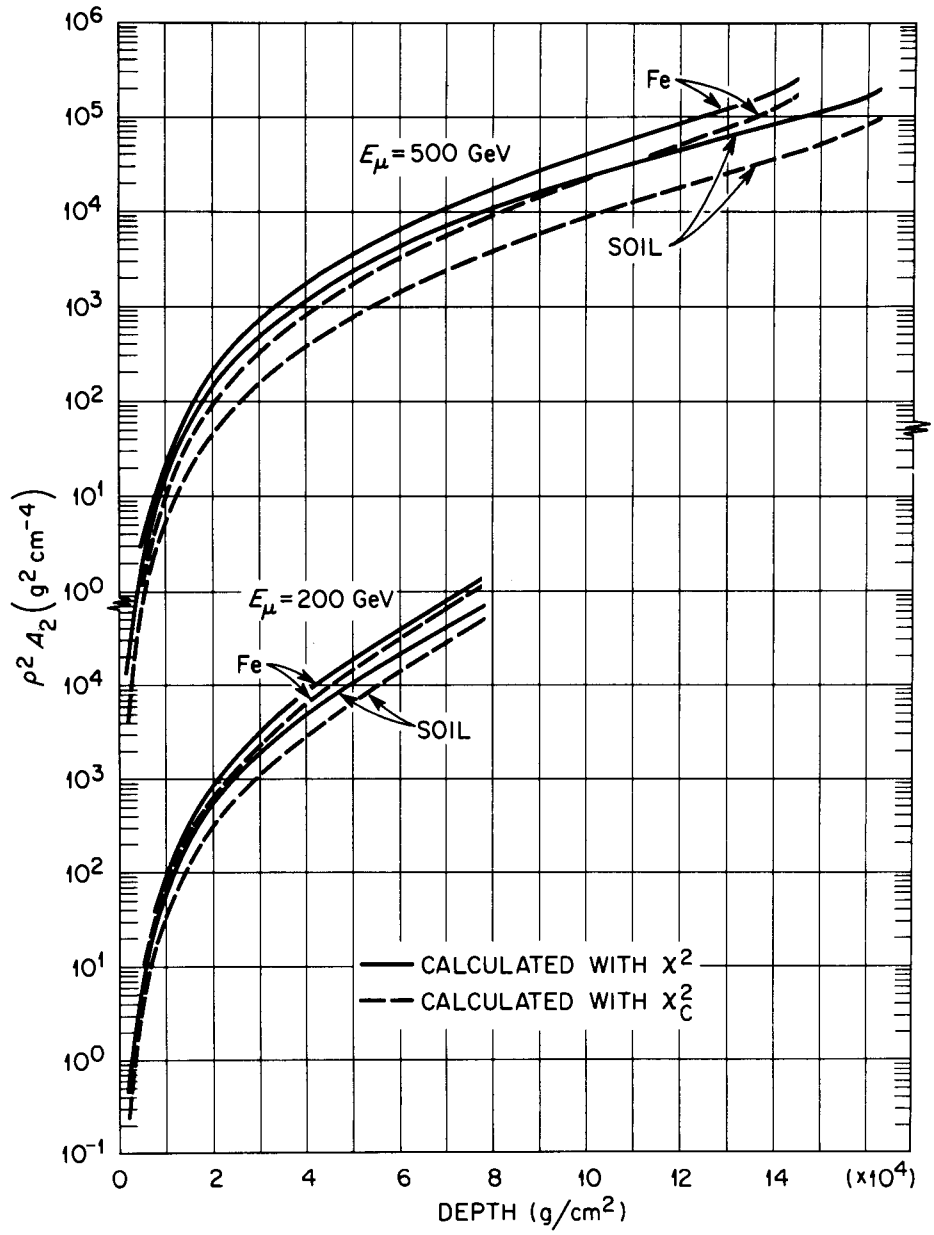

Fig. 3 The coefficient A_2 [see Eq. (4.2)] multiplied by the density squared vs depth in shield in g/cm^2.

of the angular scattering from all processes and the dashed curves that neglect the angular scattering effects of bremsstrahlung production, pair production, and nonelastic nuclear interactions.

The quantity A_2, calculated with χ^2, is shown in Fig. 4 as a function of shield depth in g/cm^2 for 200-GeV and 500-GeV muons normally incident on shields of iron and soil and on a laminated slab shield composed of 6 m of iron, followed by 357 m of soil, followed by 70 m of air,

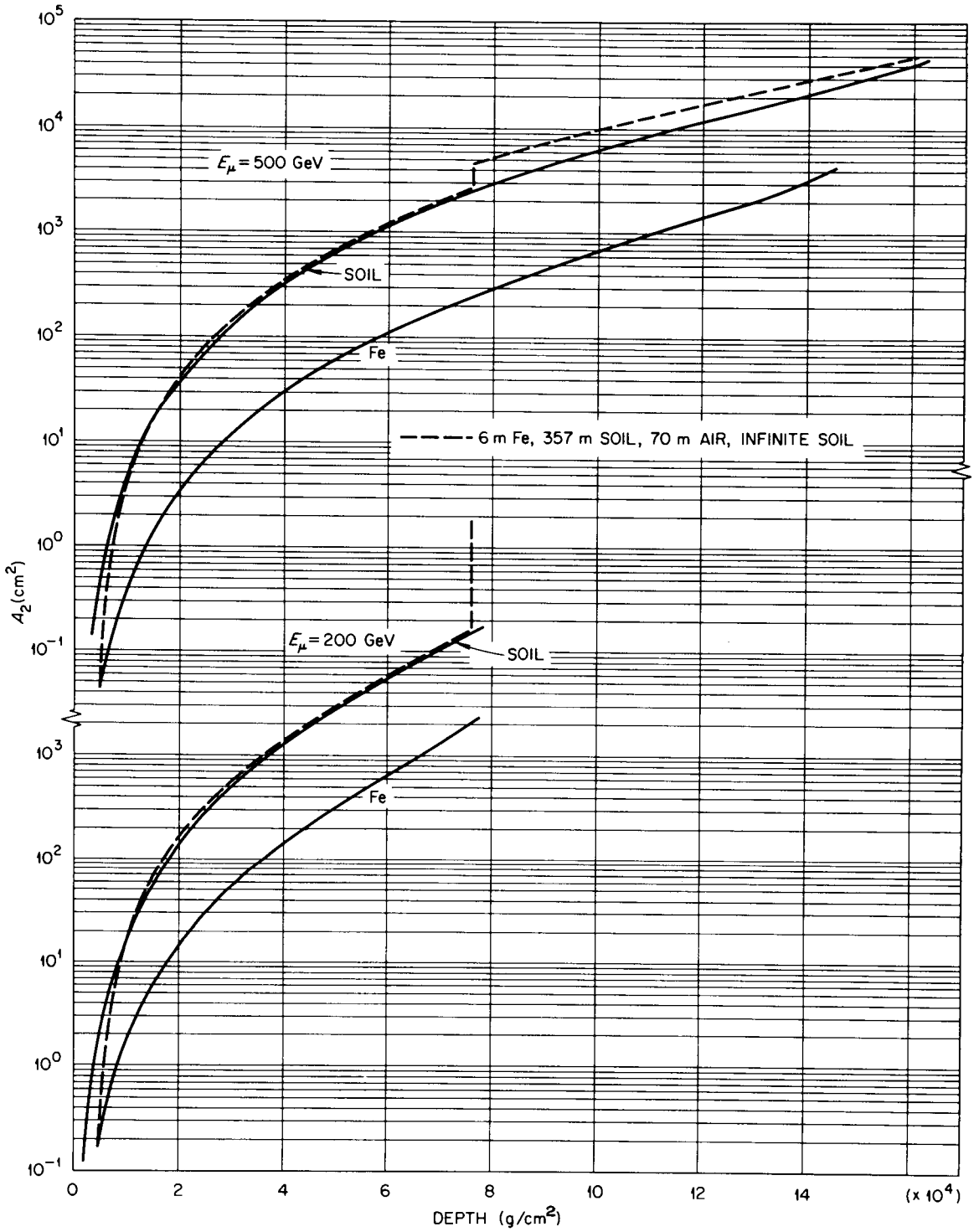

Fig. 4 The coefficient A_2 [see Eq. (4.2)] vs depth in shield in g/cm^2.

and followed by an infinite extent of soil. The iron and soil curves in Fig. 4 are the same as those in Fig. 3 except that A_2 is shown rather than $\rho^2 A_2$.

For both 200- and 500-GeV incident muons, the value of A_2 for the laminated shield case (dashed curve) is the same as the value of A_2 for iron at a shield depth of 6 m of iron (4680 g/cm^2). This must be so since the first 6 m of shield in the laminated case is iron. As the shield depth increases beyong 6 m, the dashed curves very quickly approach the soil curves and remain nearly the same as the soil curves until the air gap at 7.608×10^4 g/cm^2 is reached. The quantity A_2 for the laminated shield is larger than the A_2 for soil at depths of the order of 2×10^4 g/cm^2 and beyond due to the fact that the incident muons lose more energy in passing through 4680 g/cm^2 of iron than in passing through this amount of soil; i.e., at a given depth in g/cm^2 the muons in the laminated shield case have less energy than in the soil case. The 70-m air gap appears as a discontinuous change in A_2 because the graph is plotted against depth in g/cm^2. This change in A_2 in the air gap is due to streaming, which is correctly given by the Eyges solution (see Section 2), and would not appear as a discontinuity if the graph were plotted against depth in meters. For the 500-GeV incident muons, the dashed curve is above the soil curve at all depths beyond the air gap but becomes very nearly the same as the solid curve at the largest depths, i.e., near the range of the 500-GeV particles. Thus at very large depths in g/cm^2 the effect of the air gap on A_2, and consequently on the lateral spread of the beam, is very small. The position of the air gap was chosen so that the incident 200-GeV muons would have very low energy ($\sim$ 500 MeV) when they entered the air. There is an appreciable lateral spread of these particles as they pass through the air gap, but they are sufficiently low in energy that they stop very rapidly when they enter the soil shield after leaving the air gap. (The extension of the curve into the soil after the air gap in the 200-GeV case is not shown in the figure.)

5. SHIELDING AROUND A HIGH-ENERGY PROTON ACCELERATOR TARGET - HOMOGENEOUS SHIELDS

5.1 Geometry and muon source

Consider a proton beam interacting with a target in a geometry such as that shown in Fig. 5. It will be assumed that the target is sufficiently small that it may be approximated as a point. In this approximation, the energy-angle distribution of the pions that emerge from the target is the same as the differential production spectrum of pions,

$$\frac{d^2N_\pi}{dP_\pi d\Omega_\pi} ,$$

from a proton-nucleus collision. In the calculations presented here, this differential production spectrum is taken from the work of Trilling[27], as modified by Ranft and Borak[28], and is obtained by adding the differential production spectrum of positively and negatively charged pions.

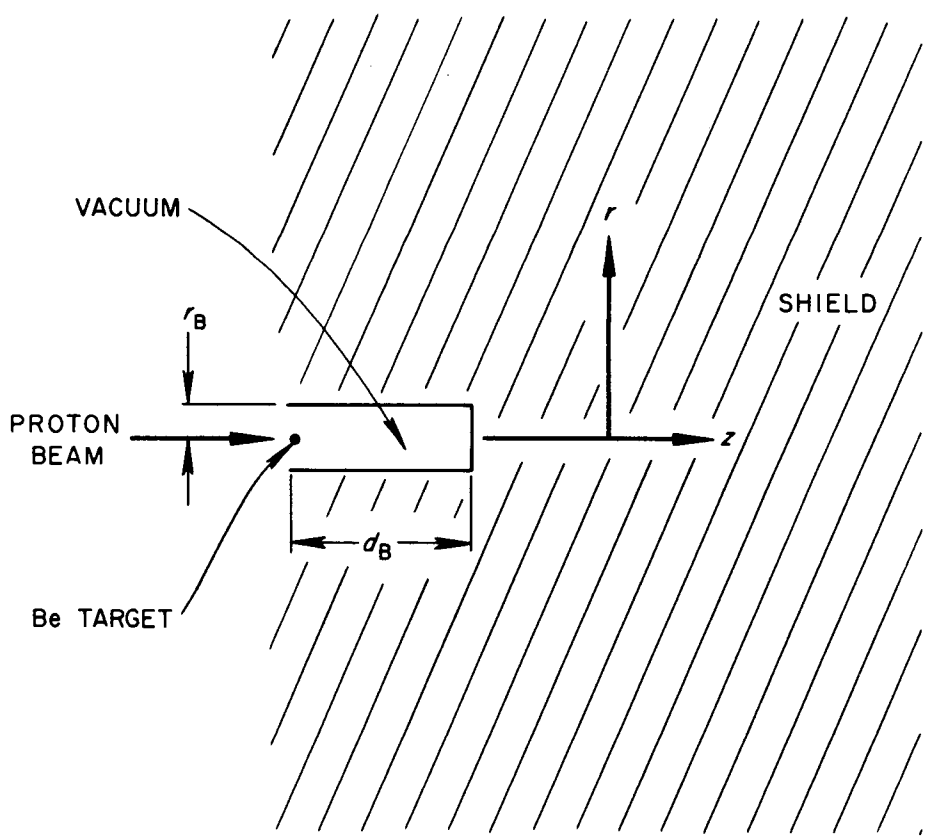

Fig. 5 Schematic diagram of target and shield.

In traveling from the target to the shield the pions may decay into muons. The probability $P_D(P_\pi, \cos\theta_\pi)$ that a pion decays into a muon before it reaches the shield may be written as

$$P_D(P_\pi,\cos\theta_\pi) = 1 - \exp\left\{-\left[\left(\frac{m_\pi}{P_\pi}\right)\frac{d_B}{\tau_\pi \cos\theta_\pi}\right]\right\} \qquad \tan\theta_\pi < \frac{r_B}{d_B} \tag{5.1}$$

$$= 1 - \exp\left\{-\left[\left(\frac{m_\pi}{P_\pi}\right)\frac{r_B}{\tau_\pi \sin\theta_\pi}\right]\right\} \qquad \tan\theta_\pi \geq \frac{r_B}{d_B} \tag{5.2}$$

where

τ_π = the lifetime of a pion at rest multiplied by the velocity of light,

and r_B and d_B are shown in Fig. 5.

When a high-energy pion decays into a muon, the angle of emission of the muon with respect to the direction of motion of the pion is small and will be neglected. That is, it is assumed that the muon from a pion decay is emitted in the direction of the motion of the pion. Under this assumption, the energy distribution of the muon $F_{\mu\pi}(E_\mu,P_\pi)$ from the decay of a pion with momentum P_π may be written[6)]

$$F_{\mu\pi}(E_\mu,P_\pi) = \frac{m_\pi^2}{P_\pi(m_\pi^2-m_\mu^2)} \qquad E_{\mu min}(P_\pi) \leq E_\mu \leq E_{\mu max}(P_\pi) \ , \tag{5.3}$$

where

$E_{\mu min}(P_\pi)$, $E_{\mu max}(P_\pi)$ = the minimum and maximum energy, respectively, of muons that may be emitted from a pion of momentum P_π. (Explicit expressions for these energies are given in Ref. 6, p. 191).

Combining Eqs. (5.1), (5.2), and (5.3) with the distribution of pions leaving the target, the distribution of muons that are incident on the shield may be written

$$S_o(E_\mu,\cos\theta_\mu) = \int_{P_{\pi min}}^{P_{\pi max}} \frac{d^2N_\pi}{dP_\pi d\Omega_\pi} \; P_D(P_\pi,\cos\theta_\mu)\; F_{\mu\pi}(E_\mu,P_\pi)\; dP_\pi \ , \tag{5.4}$$

$$P^2_{\pi max} = \left[\frac{m_\pi}{m_\mu}\right]\left\{(E_\mu + m_\mu)\left[\frac{m_\pi^2 + m_\mu^2}{2m_\pi\ m_\mu}\right] + [E_\mu(E_\mu + 2m_\mu)]^{\frac{1}{2}}\left[\frac{m_\pi^2 - m_\mu^2}{2m_\pi\ m_\mu}\right]\right\} - m_\pi^2 \ , \qquad (5.5)$$

$$P^2_{\pi min} = \left[\frac{m_\pi}{m_\mu}\right]\left\{(E_\mu + m_\mu)\left[\frac{m^2 + m_\mu^2}{2m_\pi\ m_\mu}\right] - [E_\mu(E_\mu + 2m_\mu)]^{\frac{1}{2}}\left[\frac{m_\pi^2 - m_\mu^2}{2m_\pi\ m_\mu}\right]\right\} - m_\pi^2 \ , \qquad (5.6)$$

where

$S_o(E_\mu, \cos\theta_\mu)$ = the number of muons per unit energy per unit solid angle per interacting proton in the target that are incident on the shield,

$P_{\pi min}$, $P_{\pi max}$ = the minimum and maximum pion momenta that may produce a muon with kinetic energy E_μ.

The source S_o given by Eq. (5.4) and obtained with a proton target of beryllium is used in all subsequent calculations. In addition to the explicit assumptions made above in determining S_o, there are two implicit assumptions which must be noted since neither may be entirely valid. First, in addition to the muons from pion decay, there will be some muons from kaon production and decay, and these have been neglected[1,29]. Second, there will be some muons produced by the strongly interacting particles after they enter the shield, and these muons have been neglected[1,29].

5.2 Flux and dose calculation

The solution to the muon transport equation given in Section 4 is, strictly speaking, valid only for normally incident monoenergetic muons, but it may also be assumed to be approximately valid in the case of non-normal incidence provided that z_μ and r_μ are understood to be defined with respect to the direction of incidence. To use this solution in conjunction with the source S_o, it must be written in terms of the coordinates r, z, θ_μ, $\phi_\mu - \phi$ (see Fig. 4) and averaged over the relative azimuthal angles $\phi_\mu - \phi$. This integration cannot be carried out exactly, but, using the approximations described in detail in Ref. 2, the omnidirectional flux ψ may be written

$$\psi(E_\mu,\cos\theta_\mu,z,r) = \frac{1}{4\pi\ A_2(E_\mu,z_\mu)}\ I_o\left[\frac{2(z+d_B)r\ \sin\theta_\mu\ \cos\theta_\mu}{4A_2(E_\mu,z_\mu)}\right]$$

$$\times\ \exp\left\{-\frac{1}{4A_2(E_\mu,z_\mu)}\ [r^2\ \cos^2\theta_\mu + (z+d_B)^2\ \sin^2\theta_\mu]\right\} \qquad (5.7)$$

with

$$z_\mu = \frac{z}{\cos\theta_\mu} \qquad \tan\theta_\mu < \frac{r_B}{d_B}\ , \qquad (5.8)$$

$$= \frac{z+d_B}{\cos\theta_\mu} - \frac{r_B}{\sin\theta_\mu} \qquad \tan\theta_\mu \geq \frac{r_B}{d_B}\ , \qquad (5.9)$$

where

$\psi(E_\mu,\cos\theta_\mu,z,r)$ = the omnidirectional flux at a point r,z in the shield due to a muon with kinetic energy E_μ and momentum direction defined by the polar angles θ_μ,ϕ_μ. (In obtaining Eq. (5.6), an average over the azimuthal source angle ϕ_μ has been carried out so Eq. (5.6) can be used only with an azimuthally symmetric source.)

I_o = the modified Bessel function of order zero.

The omnidirectional flux of muons, ψ_S, at a point r,z in the shield from the source S_o may be written

$$\psi_S(z,r) = 2\pi \int_{E_{min}}^{E_{max}} dE_\mu \int_o^1 d(\cos\theta_\mu)\ S(E_\mu,\cos\theta_\mu)\ \psi(E_\mu,\cos\theta_\mu,z,r)\ , \qquad (5.10)$$

where

E_{max} = the maximum muon energy that can arise from a proton non-elastic collision in the target,

$E_{min}(z)$ = the value of E_μ from Eq. (4.3) when $E_S = 0$ and $\theta_\mu = 0$.

In practice, the contribution to the integral in Eq. (5.10) at large values of $\cos\theta_\mu$ is very small, and the upper limit on the $\cos\theta_\mu$ integration may be taken to be much less than unity.

Since only the energy-integrated flux has been calculated, in principle it is not possible to calculate the dose that is dependent on the flux per unit energy. However, because the continuous slowing-down

approximation is used and because it was previously assumed that the energy loss is dependent only on z_μ, an estimate of the energy E_S that a muon with initial energy E_μ and momentum direction $\cos\theta_\mu$ will have at a point r,z may be obtained (for a homogeneous shield) from the equation

$$\int_{E_S}^{E_\mu} \frac{dE'}{S(E')} = \frac{\rho z}{\cos\theta_\mu} \qquad \tan\theta_\mu < \frac{r_B}{d_B} \tag{5.11}$$

$$= \rho\left[\frac{z+d_B}{\cos\theta_\mu} - \frac{r_B}{\sin\theta_\mu}\right] \qquad \tan\theta_\mu \geq \frac{r_B}{d_B} \quad . \tag{5.12}$$

With this estimate of the energy, the absorbed dose may be calculated as

$$D(z,r) = 2\pi \int_{E_{min}}^{E_{max}} dE_\mu \int_0^1 d(\cos\theta_\mu)\, S_o(E_\mu,\cos\theta_\mu)$$

$$\times\ \psi(E_\mu,\cos\theta_\mu,z,r)\ \rho_T S_T(E_S) \tag{5.13}$$

where

$S_T(E_S)$ = the stopping power of tissue (in $\mathrm{MeV\cdot g^{-1}\ cm^2}$) for a muon of kinetic energy E_S,

ρ_T = the density of tissue ($\mathrm{g/cm^3}$),

and E_S is to be determined in terms of E_μ and $\cos\theta_\mu$ from Eqs. (5.11) and (5.12). The stopping power of tissue for muons was obtained in the same manner as was the stopping power of iron and soil (see Section 3.1).

When D(z,r) has been calculated, contours of constant dose in the shield are determined from the equation

$$D(z,r) = \text{constant} \ . \tag{5.14}$$

5.3 Results and discussion

In the geometry shown in Fig. 5, with r_B = 15 cm and d_B = 600 cm, calculated results have been obtained for 200- and 500-GeV protons with a soil shield and for 500-GeV protons with an iron shield. Isodose contours in the iron and soil shields, respectively, for 500-GeV incident protons are shown in Figs. 6 and 7, and isodose contours in the soil

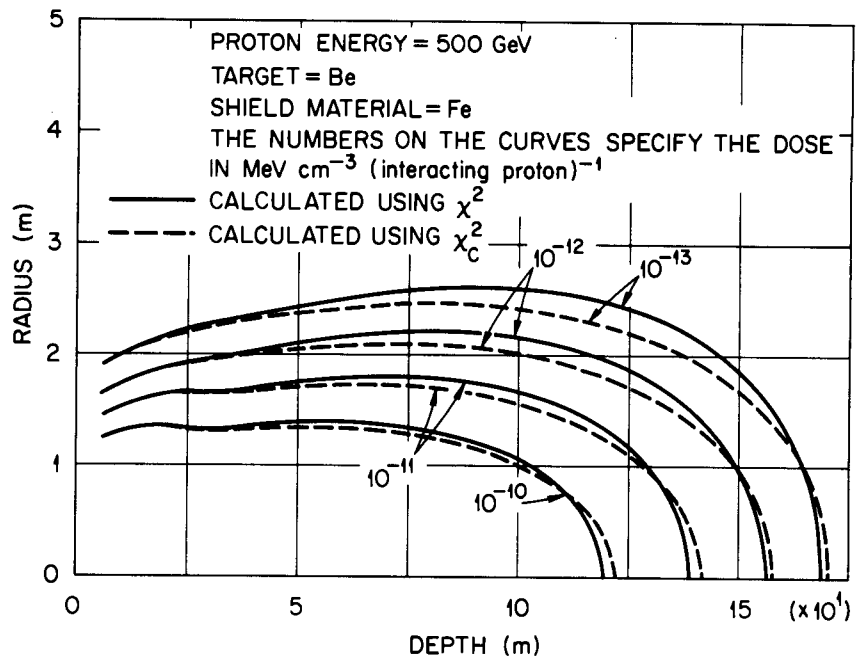

Fig. 6 Muon isodose contours in an iron shield for 500-GeV protons incident on a beryllium target.

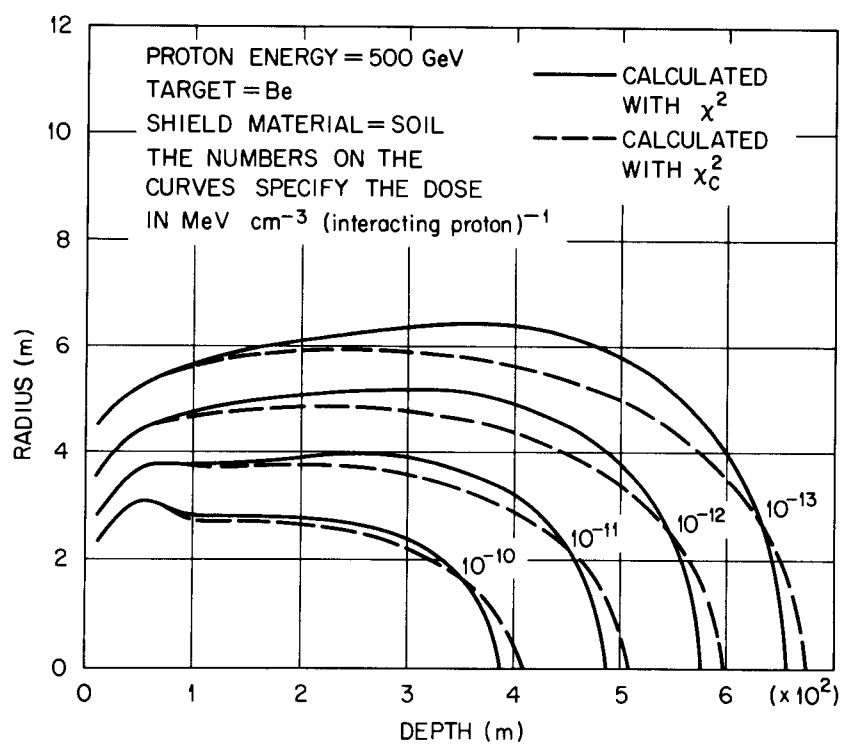

Fig. 7 Muon isodose contours in a soil shield for 500-GeV protons incident on a beryllium target.

shield for 200-GeV incident protons are shown in Fig. 8. In all of these figures, the solid curves represent the results when all angular scattering processes, Coulomb elastic scattering, bremsstrahlung production, pair production, and nonelastic nuclear interactions are considered, and the dashed curves represent the results when only the angular effects of Coulomb scattering are included. The dashed curves then correspond to the approximation made in Refs. 1, 2, and 3.

In all of the figures, the solid and dashed curves are the same at small shield depths, i.e., at small values of z, because the source muons that contribute appreciably to the dose at these depths are at energies such that $\chi^2 \simeq \chi_C^2$ (see Fig. 2). At intermediate depths in Figs. 6 and 7, the differences between the solid and dashed curves are quite small at the large dose values, i.e., at relatively small radii, but become more pronounced at the lower dose values, i.e., at the larger radii. In Fig. 8 the differences between the solid and dashed curves are small at all depths because at nearly all muon energies that can be produced by 200-GeV protons $\chi^2 \simeq \chi_C^2$. In all of the isodose contours, zero radius for a given dose occurs at a larger depth for the dashed curves than for the solid curves. This is because the portion of the curves in the vicinity of zero radius is determined by the source muons with very high energies, and these muons are scattered to larger radii when all angular scatterings are considered than when only Coulomb scattering is considered.

6. SHIELDING AROUND A HIGH-ENERGY PROTON ACCELERATOR TARGET - LAMINATED SHIELDS

In this section, isodose curves for a shield composed of layers of 6 m of iron, 357 m of soil, and 70 m of air, followed by an infinite layer of soil, are compared with those for a similar shield with the air gap omitted. Slowing down and multiple scattering from all processes are included in the computation of the lateral distribution for a given muon direction of incidence. The "width" coefficient, $A_2(E_\mu, z_\mu)$, for the shield with the air gap included was shown in Fig. 4 for initial muon energies of 500 GeV and 200 GeV.

The pion source spectrum is the same as that used in Section 5, for 500-GeV protons incident on a beryllium target, but is restricted to a narrow cone of angles (see Fig. 5) such that

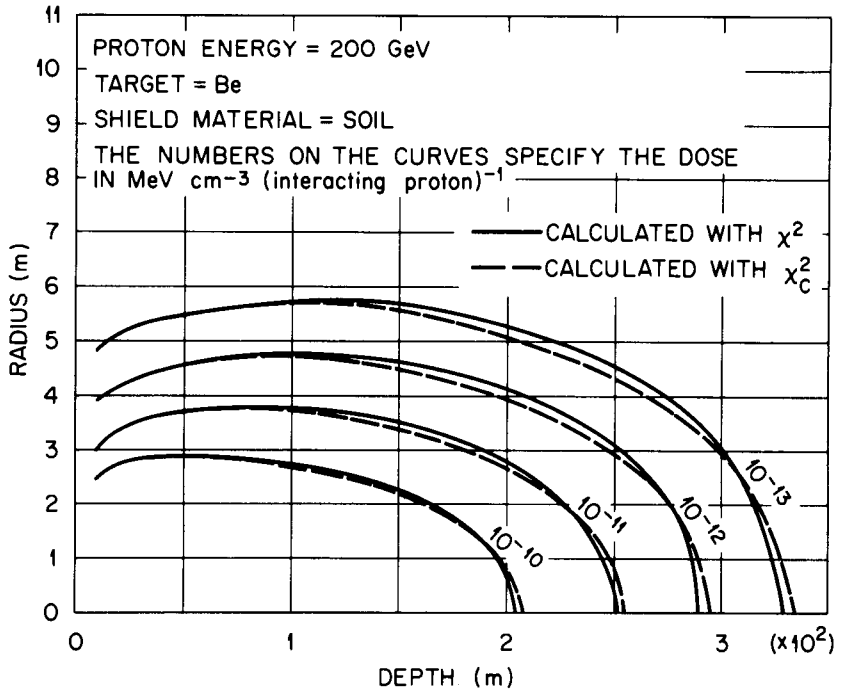

Fig. 8 Muon isodose contours in a soil shield for 200-GeV protons incident on a beryllium target.

$$\tan\theta_\mu \leq r_B/d_B \ ,$$

where d_B is the length of the pion decay space following the target and r_B its radius. For this case, $\theta_{\mu max}$ is approximately 25 mr.

The pion decay distance in direction θ_μ is taken to be $d_B/\cos\theta_\mu$, so the decay probability is that given by Eq. (5.1). This, with the source spectrum, determines the function $S_o(E_\mu,\cos\theta_\mu)$, which is the muon intensity incident on the first interface of the shield for each value of θ_μ. The first interface is a flat plane normal to the proton beam direction.

Thereafter, the muon slowing down is computed along paths in which the sequence of materials and the layer widths are taken to be the same for each value of $\theta_\mu \leq 25$ mr. The reason for this is simply computational convenience. Hence, from the point of view of slowing down along the incident muon direction, the shield geometry is roughly that of spherical shells with radii passing through the target for $\theta_\mu \leq 25$ mr. For the special cases computed here, the interface positions in each direction θ_μ are:

$z_\mu = 0$ = the first air-iron interface,

$z_\mu = z_1 = 6$ m = the iron-soil interface

$z_\mu = z_2 = 363$ m = the soil-air interface, if air gap is present,

$z_\mu = z_3 = 433$ m = the air-soil interface, if air gap is present.

The distance $z_3 - z_2$ is a distance in soil, for the comparison case.

The slowing-down energies are computed from Eq. (2.31) or Eq. (4.3). The coefficient $A_2(E_\mu, z_\mu)$ was computed by Eq. (4.2) and is also the same for each value of θ_μ.

The Eyges solution for the muon flux is used in each direction θ_μ. The lateral distribution is computed assuming that each layer of material is a slab of a given width, taken normal to the z_μ axis; i.e., that the mean-square scattering angle per unit distance depends only on z_μ and E_μ. A superposition of such solutions is used in integrating over the source distribution, as was done in Section 5 for a homogeneous shield. The error in the case of a layered shield will not be large unless the lateral deflections are large near the interfaces. This happens only in the case of air gaps in which slowing down is negligible, so the muons which might have been stopped in soil continue streaming in the direction of entry into the air gap until the next soil interface is reached. The slant streaming distances in air for large angles and the resulting lateral deflections may be different for different geometric descriptions. For the large distances used here ($z_3 = 433$ m), the error should be small.

The azimuthally averaged muon flux in a fixed plane normal to the z axis (proton direction) is given by Eq. (5.7), with Eq. (5.8),

$$z_\mu = z/\cos\theta_\mu \ ,$$

used as the approximation for $z_\mu(r,z,\theta_\mu)$ in the coefficient A_2. The same approximation for z_μ is used to compute the energy $E_S(E_\mu, z_\mu)$ of the muons in this plane, according to Eq. (4.3), when the energy-dependence of the muon stopping power in tissue is taken into account in computing the dose. The dose $D(z,r)$ is given by Eq. (5.13).

Isodose contours are shown in Fig. 9 with the radius given in meters and the depth given in g/cm^2. The solid curves show the results for the iron-soil shield with no air gap and the dashed curves show the results when the 70-m air gap beginning at a depth of 363 m is included. The

air gap appears as a discontinuity in the isodose curves because the width of the gap in g/cm^2 is very small. At depths before the air gap the two shields are identical and thus the isodose curves are identical.

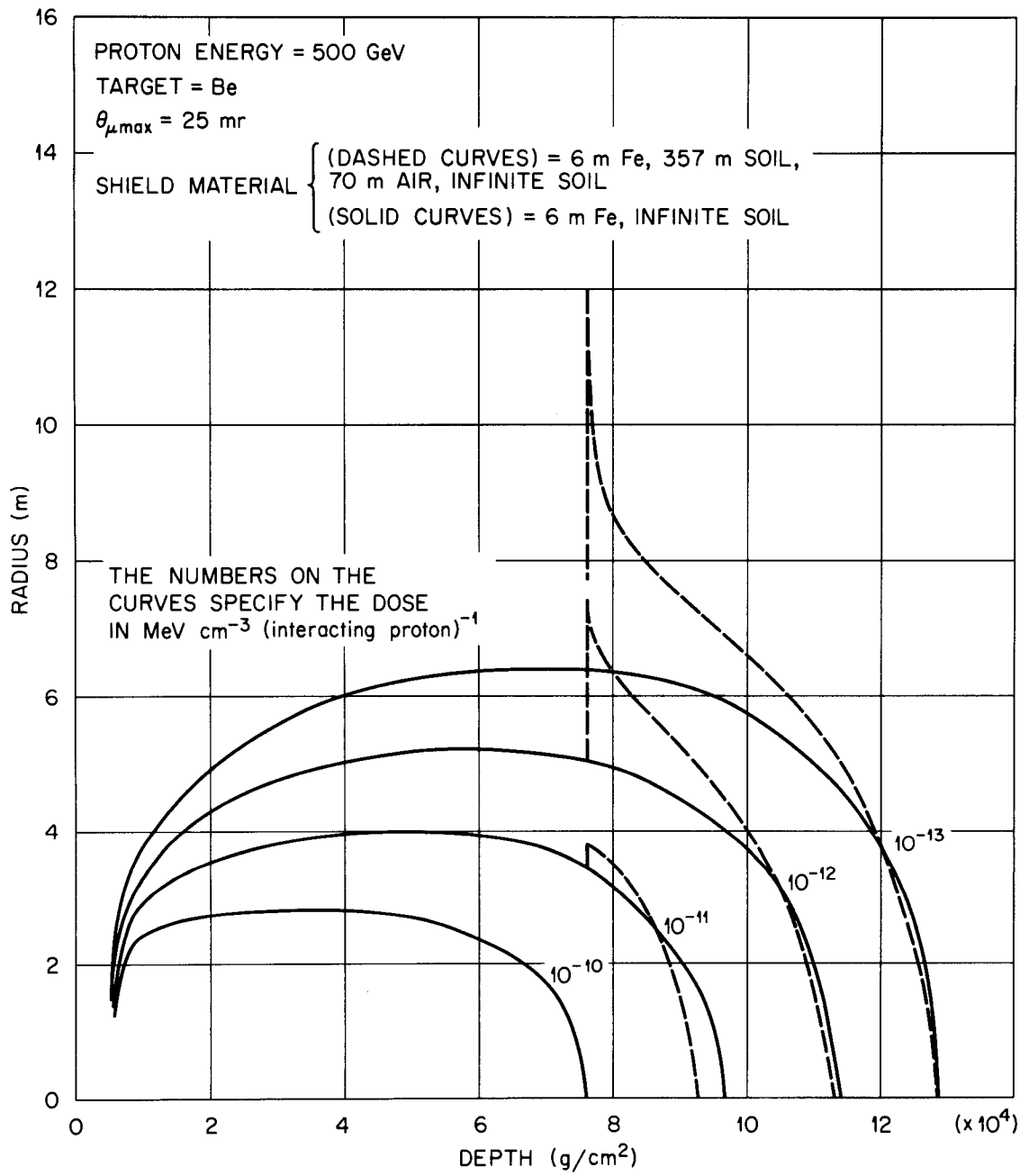

Fig. 9 Muon isodose contours in laminated shields for 500-GeV protons incident on a beryllium target.

The presence of the air gap does not greatly change the length of the shield for a given dose level since the slowing-down distance along the beam direction is unchanged. However, the streaming of the muons in the air gap greatly increases the radial extent of the soil shield necessary just beyond the air gap for a fixed dose level of 10^{-13} MeV cm^{-3} (interacting proton)$^{-1}$. For larger dose levels, the effect of the air gap on the radial extent of the shield is not nearly as great. The contour for a dose level of 10^{-10} MeV cm^{-3} (interacting proton)$^{-1}$ reaches zero radius in the soil just before the air gap, and thus for this dose level, in the case considered, the air gap has no effect on the shield.

* * *

REFERENCES

1) D. Keefe and C. M. Noble, Nucl. Instr. Meth 64, 173 (1968).

2) R. G. Alsmiller, Jr., M. Leimdorfer, and J. Barish, High-energy muon transport and the muon backstop for a 200-GeV proton accelerator, Oak Ridge National Laboratory Report ORNL-4322 (1968).

3) R. G. Alsmiller, Jr., and J. Barish, High-energy muon transport and the muon backstop for a multi-GeV proton accelerator, Oak Ridge National Laboratory Report ORNL-4386 (1969).

4) L. Eyges, Phys. Rev. 74, 1534 (1948).

5) P. J. Hayman, N. S. Palmer, and A. W. Wolfendale, Proc. Roy. Soc. London, 275, 391 (1963).

6) Bruno Rossi, High-Energy Particles, Prentice Hall, Inc., Englewood Cliffs, N. J. (1956).

7) W. T. Scott, Rev. Mod. Phys. 35, 231 (1963).

8) H. Bethe and J. Ashkin, Passage of radiation through matter, in Experimental Nuclear Physics, ed. E. Segre, Part II, John Wiley & Sons, Inc., New York (1963).

9) R. M. Sternheimer, Phys. Rev. 84, 851 (1952).

10) R. M. Sternheimer, Phys. Rev. 103, 511 (1956).

11) R. M. Sternheimer, Phys. Rev. 115, 137 (1959).

12) R. M. Sternheimer, Phys. Rev. 145, 247 (1966).

13) T. W. Armstrong and R. G. Alsmiller, Jr., Nucl. Instr. Meth. 82, 289 (1970).

14) K. Kobayakawa, Nuovo Cimento XLVII B, 156 (1967).

15) R. H. Thomas, Energy loss of high-energy muons, Lawrence Radiation Laboratory Report UCID 10010 (1964).

16) N. F. Mott and H. S. W. Massey, The Theory of Atomic Collisions, Oxford University Press, London (1949).

17) N. F. Mott, Proc. Roy. Soc. London A135, 429 (1932).

18) G. Molière, Z. Naturforsch. 2a, 133 (1947).

19) R. Hofstadter, Rev. Mod. Phys. 28, 214 (1956).

20) P. T. McCormick, D. G. Keiffer, and G. Pargen, Phys. Rev. 103, 29 (1956).

21) S. J. Biel and E. H. S. Burhop, Proc. Phys. Soc. 68, 165 (1955).

22) U. Fano, Phys. Rev. 116, 1156 (1959).

23) H. W. Koch and J. W. Motz, Rev. Mod. Phys. 31, 920 (1959).

24) J. M. Jauch and F. Rohrlich, The Theory of Photons and Electrons, Addison-Wesley, Reading, Mass. (1955).

25) M. J. Tannenbaum, Jefferson Physical Laboratory, Harvard University, Cambridge, Mass., private communication.

26) K. Daiyasu *et al.*, J. Phys. Soc. Japan 17, Supp. A-111, 344 (1962).

27) G. H. Trilling, Pion and proton fluxes from high-energy proton collisions, Lawrence Radiation Laboratory Report UCRL-16830 (1966), p. 25.

28) J. Ranft and T. Borak, Improved nucleon-meson cascade calculations, National Accelerator Laboratory Report FN-193, 1100.0 (1969).

29) 200 BeV accelerator design study, Lawrence Radiation Laboratory Report UCRL-16000 (1965).

Internal Distribution

1-3. L. S. Abbott
4. F. S. Alsmiller
5-29. R. G. Alsmiller, Jr.
30. T. W. Armstrong
31-35. J. Barish
36. H. W. Bertini
37. C. E. Clifford
38. T. A. Gabriel
39. M. P. Guthrie
40. W. E. Kinney
41. T. A. Love
42. F. C. Maienschein
43. R. W. Peelle
44. R. W. Roussin
45. R. T. Santoro
46. D. Sundberg
47. J. A. Turner
48. J. W. Wachter
49. H. A. Wright
50. W. Zobel
51. E. R. Cohen (consultant)
52. H. Feshbach (consultant)
53. H. Goldstein (consultant)
54. C. R. Mehl (consultant)
55. H. T. Motz (consultant)
56-57. Central Research Library,
58. ORNL Y-12 Technical Library, Document Reference Section
59-60. Laboratory Records Department
61. Laboratory Records ORNL RC
62. ORNL Patent Office

External Distribution

63. P. B. Hemmig, Division of Reactor Development & Technology, U. S. Atomic Energy Commission, Washington, D. C.
64. W. H. Hannum, Division of Reactor Development & Technology, U. S. Atomic Energy Commission, Washington, D. C.
65. Kermit Laughon, AEC Site Representative.
66-70. Y. Shima, Soreq Nuclear Research Center, Yavne, Israel.
71-172. Given AEC High-Energy Accelerator Shielding Distribution.*
173-174. Division of Technical Information (DTIE).
175. Laboratory and University Division (ORO).

*This distribution list is available upon request.